REFERENCE

NBS
PUBLICATIONS

A11102 247925

NAT'L INST OF STANDARDS & TECH R.I.C.
A11102247925
Hill, David A/Out-of-band response of an
QC100 .U56 NO.86-3047 1986 V19 C.1 NBS-P

NBSIR 86-3047

OUT-OF-BAND RESPONSE OF ANTENNA ARRAYS

David A. Hill
Michael H. Francis

National Bureau of Standards
U.S. Department of Commerce
Boulder, Colorado 80303

June 1986

QC
100
.U56
86-3047
1986

NBS
RESEARCH
INFORMATION
CENTER

NBSIR 86-3047

OUT-OF-BAND RESPONSE OF ANTENNA ARRAYS

David A. Hill
Michael H. Francis

Electromagnetic Fields Division
Center for Electronics and Electrical Engineering
National Engineering Laboratory
National Bureau of Standards
Boulder, Colorado 80303

June 1986

Supported by
Defense Nuclear Agency (DNA)
Alexandria, Virginia 22310

U.S. DEPARTMENT OF COMMERCE, Malcolm Baldrige, Secretary

NATIONAL BUREAU OF STANDARDS, Ernest Ambler, Director

CONTENTS

Page

Abstract....1

1. INTRODUCTION....1

2. ANTENNA ARRAY THEORY....1
    2.1 Effective Aperture....2
    2.2 Directivity Theory....3
    2.3 Directivity Calculations....6
    2.4 Impedance Mismatch....8

3. NEAR-FIELD MEASUREMENTS....9
    3.1 ULSA Measurements....9
    3.2 AWACS Measurements....10
    3.3 Sampling Considerations....10

4. CONCLUSIONS....12

5. REFERENCES....14

APPENDIX....16

OUT-OF-BAND RESPONSE OF ANTENNA ARRAYS

David A. Hill and Michael H. Francis

Electromagnetic Fields Division
National Bureau of Standards
Boulder, CO 80303

The response of antenna arrays to out-of-band frequencies has been analyzed using the effective aperture approach. An average value of effective aperture can be obtained by averaging the incidence angle and the polarization of the incidence field. Far-field patterns have also been calculated by treating the array element excitations as random variables. The randomness in the element excitations causes a decrease in directivity and an increase in sidelobe level. Out-of-band measurements of reflection coefficient and near-field response have been made on two large slotted-waveguide arrays for frequencies from 2 to 18 GHz. Both arrays are narrow band, and this is easily explained by the large impedance mismatch at out-of-band frequencies.

Key words: antenna array; directivity; impedance mismatch; near-field measurements; out-of-band response; polarization; slotted waveguide.

1. INTRODUCTION

The response of antennas to out-of-band frequencies [1-3] plays an important role in interference and jamming problems. The initial National Bureau of Standards (NBS) work in this area included an analysis of reflector antennas [4] and a comparison with previous measurements at out-of-band frequencies [5]. In this report we consider antenna arrays.

The organization of this report is as follows. Section 2 contains an analysis of antenna arrays for out-of-band frequencies. Effective aperture, directivity, and impedance mismatch are treated in detail. Section 3 contains near-field measurements at out-of-band frequencies on two large arrays of slotted waveguides. Some considerations on sampling in frequency and space are also included. Section 4 summarizes the results of this study and includes recommendations for future work.

2. ANTENNA ARRAY THEORY

In this section we analyze the receiving characteristics of antenna arrays at out-of-band frequencies. Sections 2.1 and 2.4 on effective aperture and impedance mismatch are actually applicable to arbitrary antenna types, but sections 2.2 and 2.3 are specific to antenna arrays.

2.1 Effective Aperture

The effective aperture A of an antenna is defined as the ratio of the received power to the incident power density. If we follow Tai's definition and notation, then A can be written [6]

$$A = pq \frac{\lambda^2 D(\theta,\phi)}{4\pi} , \qquad (1)$$

where p is the polarization mismatch factor, q is the impedance mismatch factor, λ is the free space wavelength, and D is the directivity of the antenna in the direction of the incident field (θ,ϕ).

The result in (1) is quite general and can be used to derive several useful results. If the antenna is polarization matched to the incident field, then p = 1. If the load impedance is conjugate matched to antenna, then q = 1. If the antenna is isotropic, then D = 1 for all θ and ϕ. In this case, (1) reduces to the well known value,

$$A = \frac{\lambda^2}{4\pi} , \qquad (2)$$

for an isotropic antenna [7].

For out-of-band frequencies, the antenna will generally not be impedance matched, and this subject will be discussed further in section 2.3. Also, the antenna polarization will not generally be matched to the incident field. If we assume that the incident field is randomly polarized, then the average value of p is [6]

$$\langle p \rangle = 1/2 , \qquad (3)$$

where < > denotes average value. In this case, (1) reduces to

$$\langle A \rangle = q \frac{\lambda^2 D(\theta,\phi)}{8\pi} . \qquad (4)$$

This is probably the most useful form for out-of-band calculations because it allows us to include the frequency dependence of q and the angular dependence of D. However, if we choose to average D over the incidence angles θ and ϕ, then we obtain

$$\langle D \rangle = 1 . \qquad (5)$$

This yields the following simple expression for <A>

$$\langle A \rangle = q \frac{\lambda^2}{8\pi} . \qquad (6)$$

For complicated antennas, it is usually not possible to compute q at out-of-band frequencies, and q must be measured [8]. For cases where the antenna feed is multimoded, each mode can be treated as a separate antenna. An open-ended waveguide example is shown in the Appendix.

2.2 Directivity Theory

In this section we analyze the far-field pattern of antenna arrays at out-of-band frequencies. Although we are interested primarily in the receiving case, we assume that the antenna array is reciprocal and that the receiving and transmitting patterns are the same. Thus we can treat the transmitting case, which is more convenient for analysis. For large arrays operating at out-of-band frequencies, the array element excitations have large uncertainties and are best represented as random variables [3]. Thus we require a statistical analysis, and some of the required statistical antenna theory has already been developed [9]. Much of the earlier work on statistical antenna theory dealt with the effect of random errors in array construction and feed networks [10-13]. In the out-of-band case the randomness in the element excitations is actually due to our lack of knowledge of the out-of-band characteristics of the components in the feed system and the array elements.

As a starting point, we follow the analysis of Gilbert and Morgan [12]. The power pattern $\phi(\bar{u})$ of an antenna array of identical elements can be written

$$\phi(\bar{u}) = s^2(\bar{u}) \left|f(\bar{u})\right|^2 , \tag{7}$$

where $s^2(\bar{u})$ is the element power pattern, $f(\bar{u})$ is the array factor, and $\bar{u}$ is a unit vector representing a direction in space. For an array of N elements, the array factor is

$$f(\bar{u}) = \sum_{n=1}^{N} A_n \exp(-ik\bar{R}_n \cdot \bar{u}) , \tag{8}$$

where k is the wavenumber ($=2\pi/\lambda$), A_n is the excitation coefficient of the nth element, $\bar{R}_n$ is the position vector of the nth element, and the time dependence is $\exp(-i\omega t)$.

We now assume that at out-of-band frequencies the excitation coefficients have some random scatter about their mean or expected values, and we can write them as [12]

$$A_n = a_n + \alpha_n , \tag{9}$$

where a_n is the expected value of A_n and the α_n's are independent random complex variables with zero mean. Gilbert and Morgan [12] assumed that the position vectors $\bar{R}_n$ were also random in order to model construction errors, but we will not consider this case. The expected or mean value of the power pattern $\langle\Phi(\bar{u})\rangle$ can be written

$$\begin{aligned}\langle\Phi(\bar{u})\rangle &= s^2(\bar{u})\ \langle|f(\bar{u})|^2\rangle \qquad (10)\\ &= s^2(\bar{u})\ [|f_0(\bar{u})|^2 + \sum_{n=1}^{N} \langle|\alpha_n|^2\rangle] ,\end{aligned}$$

where f_0 is the mean value of the array pattern

$$f_0(\bar{u}) = \sum_{n=1}^{N} a_n \exp(-ik\bar{R}_n\cdot\bar{u}) . \qquad (11)$$

In (10) we have assumed that the element power pattern $s^2(\bar{u})$ is not random. The expected value of the power pattern in (10) depends only on the expected value of $|\alpha_n|^2$, and we do not need to know the detailed statistics of α_n unless we wish to know the statistics of Φ. If we assume that the real and imaginary parts of α_n are Gaussian with zero mean, then Φ has a modified Rayleigh distribution [10].

Following Gilbert and Morgan [12], we assume that the random and deterministic parts of A_n are related by

$$\langle|\alpha_n|^2\rangle = \varepsilon^2|a_n|^2 , \qquad (12)$$

where ε is independent of n. If we substitute (12) into (10), then we obtain

$$\langle\Phi(\bar{u})\rangle = s^2(\bar{u})\ [|f_0(\bar{u})|^2 + \varepsilon^2 \sum_{n=1}^{N} |a_n|^2] . \qquad (13)$$

In order to do any out-of-band calculations, we need to know how ε depends on frequency. For a well designed array we know that ε is small at the design frequency f_0. Also, we know from limited measurements and from the out-of-band characteristics of feed system components [3] that ε increases as the frequency departs from the design frequency. Consequently we postulate that ε is proportional to the difference between the actual frequency f and the design frequency

$$\varepsilon = c \frac{f - f_0}{f_0} , \tag{14}$$

where c is a constant on the order of unity. The frequency dependence of ε in (14) can be modified for cases where a better knowledge of ε is available. Also, it is possible to treat the case where the element pattern is random [9], but we will not consider this case.

So far we have considered only the relative power pattern $\Phi(\bar{u})$. If we wish to compute directivity, we need to normalize $\Phi(\bar{u})$ to the total radiated power. For the deterministic case ($\varepsilon = 0$), the directivity $D_0(\bar{u})$ can be written

$$D_0(\bar{u}) = \Phi_0(\bar{u})/[\frac{1}{4\pi} \int \Phi_0(\bar{u})\, d\Omega] , \tag{15}$$

where $\Phi_0(\bar{u}) = s^2(\bar{u})\ |f_0(\bar{u})|^2$.

The integration in (15) is over all solid angles, and $d\Omega$ is the differential of solid angle. For the random case ($\varepsilon \neq 0$), a convenient definition of directive gain $D(\bar{u})$ is [12]

$$D(\bar{u}) = \langle\Phi(\bar{u})\rangle/[\frac{1}{4\pi} \int \langle\Phi(\bar{u})\rangle\, d\Omega] . \tag{16}$$

Strictly speaking, (16) is not correct because it assumes that the expected value of the ratio is equal to the ratio of the expected values [14]. However, (16) is a useful expression because it is generally accurate and is fairly easy to compute [12].

If we substitute (13) and (15) into (16) and perform some algebra, we obtain

$$D(u) = \frac{D_0(\bar{u}) + [s^2(\bar{u})/I_\Phi]\varepsilon^2 \sum_{n=1}^{N} |a_n|^2}{1 + (I_s/I_\Phi)\varepsilon^2 \sum_{n=1}^{N} |a_n|^2} . \tag{17}$$

The integrals I_s and I_Φ are given by

$$I_s = \frac{1}{4\pi} \int s^2(\bar{u})\, d\Omega \quad \text{and} \quad I_\phi = \frac{1}{4\pi} \int \Phi_0(\bar{u})\, d\Omega \neq 0 \ . \tag{18}$$

In general the evaluation of (17) is rather tedious because of the summation over n and the two integrations over solid angle Ω. However, there are two fairly simple limits of interest. At the design frequency when $\varepsilon = 0$, we have

$$D(\bar{u})\Big|_{\varepsilon=0} = D_0(\bar{u}) \ . \tag{19}$$

This is simply the gain for the deterministic case as given by (15). When the frequency is well above band and ε approaches ∞, we have

$$D(\bar{u})\Big|_{\varepsilon=\infty} = s^2(\bar{u})/I_s \ . \tag{20}$$

This is the directive gain of a single element where the array pattern has become isotropic.

2.3 Directivity Calculations

The expression for $D(\bar{u})$ in (17) is the primary result of the previous section, and specific array results can be calculated if the element weightings, the element pattern, and the appropriate value for c are known. To illustrate the effects that occur at out-of-band frequencies, we consider the example of a rectangular planar array of magnetic dipole elements as shown in figure 1. The number of elements N is $N_x N_y$, the x spacing is d_x, and the y spacing is d_y. We choose the planar array geometry because it is so common and the magnetic dipole element because it is a simple model for a small slot as in a slotted waveguide array [15].

We first consider the element pattern. It is easy to show that the power pattern of a magnetic dipole on a ground plane is

$$s^2(\bar{u}) = \begin{cases} \cos^2\phi + \cos^2\theta \sin^2\phi \ , & \theta < \pi/2 \\ 0 \ , & \theta > \pi/2 \end{cases} \tag{21}$$

The elevation angle θ and the azimuthal angle ϕ are defined in figure 1. By substituting (21) into (18), we can calculate I_s

$$I_s = \frac{1}{4\pi} \int_0^{2\pi} \int_0^{\pi/2} (\cos^2\phi + \cos^2\theta \sin^2\phi) \sin\theta \, d\theta \, d\phi = 1/3 \ . \tag{22}$$

From (21) and (22), we see that the directivity of a magnetic dipole on a ground plane is 3 (or 4.77 dB), which is twice that of a magnetic or electric dipole in free space.

For simplicity we consider a uniform broadside array ($a_n = 1$ for all n). Then the required sum in (17) is

$$\sum_{n=1}^{N} |a_n|^2 = N = N_x N_y \ . \tag{23}$$

The mean value of the array pattern is

$$f_0(\bar{u}) = \sum_{n_x=0}^{N_x-1} \sum_{n_y=0}^{N_y-1} \exp(-ikn_x d_x \sin\theta\cos\phi)\exp(-ikn_y d_y \sin\theta\sin\phi) \ , \tag{24}$$

where $\bar{u} = \hat{x}\sin\theta\cos\phi + \hat{y}\sin\theta\sin\phi + \hat{z}\cos\theta$ and $\hat{x}$, $\hat{y}$, and $\hat{z}$ are unit vectors. The summations in (24) can be performed analytically, and the square of the array pattern can be written

$$|f_0(\bar{u})|^2 = N^2 \left[\frac{\sin(N_y \gamma_y/2)}{N_y \sin(\gamma_y/2)}\right]^2 \left[\frac{\sin(N_x \gamma_x/2)}{N_x \sin(\gamma_x/2)}\right]^2 \ , \tag{25}$$

where $\gamma_y = kd_y \sin\theta\sin\phi$ and $\gamma_x = kd_x \sin\theta\cos\phi$. The evaluation of I_Φ as defined in (18) is generally tedious, but if we approximate $s^2(\bar{u})$ by unity and $\sin\theta$ by θ in the vicinity of the main beam where θ is small, then I_Φ can be evaluated analytically as shown by Kraus [7, p.121]

$$I_\Phi = \frac{N\lambda^2}{4\pi d_y d_x} \ . \tag{26}$$

We now have expressions for all of the quantities required for evaluation of the directivity in (17).

We consider first a square array example with the following parameters: $N_x = N_y = 10$, $d_x = d_y = \lambda_0/2$, and $f = 2f_0$, where λ_0 and f_0 are the design wavelength and frequency. In figure 2 we show the directivity in the plane $\phi = 0$ for various values of c. Since the element pattern is isotropic ($s^2 = 1$) in that plane, we are seeing the array pattern. The pattern for c = 0 is as expected for a uniform array with no randomness in the element weightings. There are nulls at $N_x \gamma_x/2$ equal to integeral multiples of π, and the first sidelobe is 13 dB below the main beam. As c is increased, the directivity decreases, and the nulls are filled in. This behavior is consistent with some of the results of Shifrin [9]. As c approaches infinity, the directivity approaches that of a single element as shown by (20). The curve for c = 5.0 is starting to show that behavior, and the directive gain for large $N_x \gamma_x/2$ is approximately that of a single element (4.77 dB). The difficult problem of choosing the appropriate value of c for a specific array would be best answered experimentally. In the absence of experimental results, a value of c near unity appears to be a reasonable choice.

For our second example, we consider a large rectangular array with the following parameters: $N_x = 120$, $N_y = 20$, $d_x = d_y = \lambda_0/2$, and $c = 1$. These parameters are close to those of the ultra low sidelobe array (ULSA) [16] which was measured on the NBS near-field antenna range as described in the following section. The design wavelength is approximately 10 cm, and the array dimensions are approximately 1 m by 6 m. The directivity in the plane $\phi = 0$ is shown in figure 3. The curve at the design frequency ($f = f_0$) is again the curve for a uniform array with nulls at $N_x\gamma_x/2$ equal to integer multiples of π. The above-band curve ($f = 4f_0$) shows a reduced gain, filled-in nulls, and a nearly constant level at large values of $N_x\gamma_x/2$. The constant level is the element directivity (4.77 dB) in the plane $\phi = 0$. The array has no grating lobes at the design frequency, but there can be grating lobes at above-band frequencies where either $\gamma_x/2$ or $\gamma_y/2$ equal integeral multiples of π as indicated by (25). However, the level of the grating lobes will be reduced just as the level of the main beam is reduced for $f = 4f_0$ in figure 3. In figure 4 we show the directivity of the same array as a function of frequency. If we neglect the randomness of the array ($c = 0$), then the directivity increases as f^2. However, when the randomness is included ($c = 1$), the directivity decreases with frequency and approaches the directivity of a single element.

Both of our examples in this section have considered a broadside array with uniform element weighting. In practical applications, the elements could have a linear phase shift for beam steering or some other weighting, such as Dolph-Chebyshev for low sidelobes [17]. In either case, the qualitative effect of randomness of element weighting at out-of-band frequencies will be the same as in the uniform array examples. The directivity will decrease, the pattern nulls will fill in, and the distant sidelobe level will rise. A close examination of (17) shows that these effects occur regardless of the particular form of the weighting coefficients a_n.

2.4 Impedance Mismatch

Tai [6] gives the following expression for the impedance mismatch factor q

$$q = \frac{4RR_L}{(R + R_L)^2 + (X + X_L)^2}, \tag{27}$$

where $Z = R + iX$ = antenna impedance and $Z_L = R_L + iX_L$ = load impedance. This expression is in agreement with that of Kraus [7, ch. 3] for the case of a lossless antenna. When the antenna has both loss resistance R_l as well as radiation resistance R_r, it is most convenient to combine impedance mismatch and resistive loss in the following expression for q,

$$q = \frac{4R_r R_L}{(R_r + R_l + R_L)^2 + (X + X_L)^2} . \tag{28}$$

If both the antenna loss resistance R_l and the load reactance X_L are zero, then (28) can be written

$$q = \frac{4RR_L}{(R + R_L)^2 + X^2} = 1 - |\Gamma|^2 , \tag{29}$$

where Γ is the input reflection coefficient of the antenna when R is the real characteristic impedance of the transmission line or waveguide feed. Since the magnitude of Γ can be measured, q is easily determined from (29). There is no need to measure the input resistance and reactance of the antenna. The main restrictions on (29) are that the antenna resistive losses must be negligible and the transmission line or waveguide feed must be single moded at the antenna terminals. Some measurements of reflection coefficient are shown in the following section.

3. NEAR-FIELD MEASUREMENTS

In this section we present the results of near-field measurements on two large slotted waveguide arrays, ULSA and AWACS. In all cases, we transmitted with the large array and received with a small probe. Reference [16] contains a discussion of the design of ULSA and AWACS and photographs of both arrays.

3.1 ULSA Measurements

In June 1985, the NBS acquired a new receiver in order to do swept frequency measurements with the near-field range. At that time a slotted waveguide array, ULSA [16], was on the near-field range for a regular near-field measurement. In order to test the receiver, the opportunity was taken to perform some swept frequency measurements at selected points in the near field. These measurements were taken over the frequency range of 2-10 GHz.

Some sample results are shown in figures 5 and 6. Figure 5 data were acquired with the probe at the center of the ULSA while figure 6 data were acquired at a position 25 cm below the center of the ULSA. Both sets of data were acquired using the same S-band open-ended waveguide probe that was used in the regular near-field measurement. In both cases the probe was located 65 cm from the plane of the array.

The character of both figures 5 and 6 is similar in that they both have a low frequency cutoff at about 2.5 GHz. This corresponds to the cutoff for the slotted waveguide of the ULSA. The response at higher frequencies is seen to decay to a level which is about 20 dB below the maximum in-band response.

3.2 AWACS Measurements

Swept frequency measurements for the AWACS were performed over the frequency range 2-18 GHz using a wideband horn probe with good response over this entire frequency range. The swept frequency measurements determined the amplitude and phase of the output at the receiver relative to the input at the transmitter as a function of frequency for each point of measurement in the near field. Measurements were made at the center of the AWACS array, 30 cm above and below the center, 61 cm below the center, 89 cm to one side of the center, and 178 cm to one side of the center. The probe was always located 35 cm from the plane of the array. Typical swept frequency results are shown in figure 7 (for the array center) and figure 8 (for 89 cm to one side of center). It can be seen from these results that the AWACS like the ULSA is narrow band. The low frequency cutoff corresponds very nearly to the cutoff of the slotted waveguide. The low response at higher frequencies is due to the large input reflection coefficient (see figure 9) which is nearly 1.0 or 0 dB.

If a Fourier transform is done on the swept frequency response, the impulse response of the antenna can be obtained. These results are found in figures 10 and 11. Time equal to zero corresponds to the signal at the input. The peak response is at 50 ns and correlates well with the time required for the signal to travel the length of the antenna and then to the probe. A secondary peak is seen at about 80 ns and is believed to be due to part of the signal reflecting off the antenna termination.

If we examine the swept frequency results we see there are two small peaks in the antenna response just above band at 3.83 GHz and 3.94 GHz. They are about 10 dB below the antenna's peak response. A one dimensional near-field measurement was made at 3.94 GHz and compared to the in-band results. The 3.94 GHz results are found in figure 12 (near field) and figure 13 (far field). The near field at 3.94 GHz is much more skewed than the in-band result. The far-field main beam at 3.94 GHz is much closer to being steered on-axis than is the in-band far-field main beam. The location of the main beam in both cases is in good agreement with the theory of slotted waveguide arrays [15]. The sidelobes at 3.94 GHz are slightly higher than the in-band sidelobes, and this is in agreement with (17).

3.3 Sampling Considerations

The measurements on ULSA and AWACS in the previous sections provide a great deal of information on the out-of-band response of these arrays, but we need to examine sampling requirements for complete and efficient characterization. In out-of-band problems, we do not require precise measurements of far-field patterns and frequency response, but we would like to be sure that we do not miss any major features, such as peaks in the frequency response or major lobes in the far-field pattern. Since large arrays at above-band frequencies have a large electrical size, we would also like to be efficient in taking the measurements.

We first consider frequency sampling. This is most easily done by examining the frequency dependence of the input reflection coefficient Γ. This quantity is related to the impedance mismatch as shown by (29). It is generally difficult to derive an expression for Γ for large phased arrays at out-of-band frequencies, but we can expect that Γ can be represented approximately in the form,

$$\Gamma \approx \sum_n B_n \exp(i2kL_n) . \tag{30}$$

Here B_n represents a normalized field scattered from some nth point on the antenna, and L_n represents the path length from the nth point back to the feed point. For example, the nth point could be a slot in a slotted waveguide array, and L_n would be the distance from that slot to the feed point. In such a case the energy could travel either along the exterior of the antenna or back down the waveguide. The form of B_n is unknown, but we expect that B_n will be slowly varying with frequency compared to the exponential factor in (30). The most rapid frequency variation in (30) will come from the exponential with the longest path length L. If we replace k by $2\pi f/v$, where v is the free space velocity of light, then the minimum sampling increment in frequency Δf is given by

$$4\pi \Delta f L/v = \pi \quad \text{or} \quad \Delta f = v/(4L) . \tag{31}$$

For example, if we consider the ULSA where L is approximately the length of the waveguide sections ($\approx$ 6 m), then $\Delta f \approx 12.5$ MHz. This value is in agreement with the rapid variations for both the ULSA and AWACS in figures 5-9. Although the expression in (31) was derived for the input reflection coefficient, a similar expression can be derived for sampling the near field where 2L is replaced by a path difference that is less than L. Thus the input reflection coefficient controls the sampling requirement, and it depends primarily on the size of the array. Details of the array, such as the element type or spacing, affect B_n in (30), but not Δf in (31).

A related sampling issue is the spatial sampling requirement for a fixed frequency. The planar near-field sampling requirement for calculation of the far-field pattern is well known [18], and the planar sample spacings are

$$\Delta x = \Delta y \leqq \lambda/2 . \tag{32}$$

If the requirement is that peaks in the near-field response are not missed, then the spacings can be somewhat greater than $\lambda/2$ as shown by geometrical considerations. Note that the distance between the peaks and valleys of the small ripples in figure 12 is just slightly greater than $\lambda/2$. In any case, the near-field response of large arrays at above-band frequencies requires an enormous number of samples.

The most efficient out-of-band measurement is probably input reflection coefficient because it yields the mismatch factor and the average effective aperture as given by (6). This will not yield any pattern information, but approximate principal plane patterns could be obtained from near-field centerline measurements as shown in figures 12 and 13. For such measurements it would be logical to choose frequencies where the input reflection coefficient is small.

4. CONCLUSIONS

The response of antenna arrays has been studied theoretically and experimentally. The effective aperture A is the most useful receiving characteristic in interference calculations, and in general A depends on incidence angle, polarization, and the load impedance. It is possible to average over incidence angle and polarization to obtain an average value as in (6). However, it is difficult to calculate the impedance mismatch factor at out-of-band frequencies, and this factor (or the reflection coefficient) must generally be measured. A typical experimental result for the reflection coefficient of the AWACS is shown in figure 9.

When pattern information is needed, then the directivity must be computed or measured. Accurate values of the element excitations are not generally known at out-of-band frequencies, and in section 2.2 the element excitations are treated as random variables. An expression for the expected value of the directive gain has been derived, and some far-field patterns are computed in section 2.3. The effects of the randomness in the element excitations are to decrease the directivity, to fill in the pattern nulls, and to raise the sidelobe levels.

Near-field measurements on two large slotted waveguide arrays, ULSA and AWACS, are shown in section 3. It is not possible to do a detailed comparison with the theory, but the qualitative trends are consistent with the theory. The narrow band nature of both arrays is evident in the measurements, and this property is most easily determined by doing a swept-frequency measurement of the antenna reflection coefficient. Near-field measurements for far-field patterns are very time consuming for large arrays at out-of-band frequencies, but approximate principal plane patterns can be obtained from centerline measurements. Some examples are shown in figures 12-15.

A number of extensions to this work would be useful. Other antenna arrays with different types of elements could be studied experimentally at out-of-band frequencies. The slotted waveguides which were studied here had sharp cutoffs below band because the waveguides were cut off. It would be interesting to do measurements on another type of array that did not use a waveguide feed and did not have a low frequency cutoff. Input reflection measurements should have high priority, and some near-field measurements and far-field calculations could be done. The pulse response of general antennas could be studied theoretically and experimentally. Some near-field pulse responses were synthesized for the AWACS as shown in figures 11 and 12. It would be useful to study the feasibility of computing the far-field pulse response of antennas from near-field pulse data (real or synthesized).

5. REFERENCES

[1] Lind, W.R. Out of band performance of antennas. Moore School of Electrical Engineering Report No. 65-18; 1965.

[2] Levinson, D.S. Transmission-line measurement techniques. Rome Air Development Center Technical Report No. RADC-TR-65-187; 1965.

[3] Cown, B.J.; Cain, F.L.; Duffy, E.G. Statistical prediction model for EMC analysis of out-of-band phased array antennas. IEEE Trans. Electromag. Compat., EMC-18: 163-170; 1976.

[4] Hill, D.A. Out-of-band response of reflector antennas. Nat. Bur. Stand. (U.S.) Interagency Report 85-3021; 1985.

[5] Cown, B.J.; Ryan, C.E.; Weaver, E.E. Antenna pattern measurements to characterize the out-of-band behavior of reflector antennas. Georgia Institute of Technology, Engineering Experiment Station, Report ECAC-TR-83-003; 1983.

[6] Tai, C.T. On the definition of the effective aperture of antennas. IEEE Trans. Ant. Propagat. AP-9: 224-225; 1961.

[7] Kraus, J.D. Antennas. New York: McGraw-Hill; 1950.

[8] Engheta, N.; Lee, K.S.H.; Yang, F.C.; Madle, P. Archimedean spiral antenna. Dikewood Memo Series on HPM Generic Coupling; 1985.

[9] Shifrin, Y.S. Statistical antenna theory. Boulder: Golem Press; 1971.

[10] Ruze, J. The effect of aperture errors on the antenna radiation pattern. Suppl. Nuovo Cimento, 9: 364-380; 1952.

[11] Bailin, L.L.; Ehrlich, M.J. Factors affecting the performance of linear arrays. Proc. IRE, 41: 235-241; 1953.

[12] Gilbert, E.N.; Morgan, S.P. Optimum design of directive antenna arrays subject to random variations. Bell Sys. Tech. J., 34: 637-663; 1955.

[13] Elliott, R.S. Mechanical and electrical tolerances for two-dimensional scanning antenna arrays. IRE Trans. Ant. Propagat., AP-6: 114-120; 1958.

[14] Ott, R.H.; Dybdal, R.B. Statistics for the directivity of an antenna array. Aerospace Corporation, Report ATR-84(8502)-1; 1984.

[15] Compton, R.T.; Collin, R.E. Slot Antennas. in Antenna Theory (ed. Collin, R.E.; Zucker, F.J.). New York: McGraw-Hill; 1969.

[16] Schrank, H.E. Low sidelobe phased array antennas. IEEE Antennas and Propagation Society Newsletter, 25(2): 5-9; 1983.

[17] Dolph, C.L. A current distribution for broadside arrays which optimizes the relationship between beam width and side-lobe level. Proc. IRE, 34: 335-348; 1946.

[18] Kerns, D.M. Plane-wave scattering-matrix theory of antennas and antenna-antenna interactions. Nat. Bur. Stand. (U.S.) Monograph 162; 1981.

[19] Brownell, F.H. Extended asymptotic eigenvalue distributions for bounded domains in n-space. J. of Math. and Mech., 6: 119-166; 1957.

APPENDIX MULTIMODE ANTENNA EXAMPLE

For multimode antennas, (1) can be generalized to

$$A = \frac{\lambda^2}{4\pi} \sum_{m=1}^{M} p_m q_m D_m(\theta,\phi) \; , \tag{A1}$$

where M is the number of modes and subscript m denotes the properties of the mth mode. For the open-ended waveguide example, we assume that each mode is matched ($q_m = 1$). If we assume that the incident field is randomly polarized and we average over all incidence angles, then (A1) becomes

$$\langle A \rangle = M \frac{\lambda^2}{8\pi} \; . \tag{A2}$$

For an open-ended waveguide, M is the number of propagating modes. In general, M depends on the shape of the waveguide cross section and the frequency in a rather complicated manner. However, if the cross-sectional dimensions of the waveguide are electrically large, then M has a fairly simple asymptotic value [19],

$$M \approx \frac{2\pi S}{\lambda^2} \; , \tag{A3}$$

where S is the cross-sectional area of the waveguide as shown in figure 16. It is easy to check (A3) for the case of a rectangular waveguide, but it is more difficult for other shapes, such as circular. If we substitute (A3) into (A2), then <A> reduces to

$$\langle A \rangle \approx S/4 \; . \tag{A4}$$

The result in (A4) can also be derived directly by geometrical optics. If we ignore edge diffraction, then the effective aperture is independent of polarization and is approximately the projected waveguide area [4],

$$A \approx \begin{cases} S\cos\theta \; , & \theta \leqq \pi/2 \\ 0 \; , & \pi/2 < \theta < \pi \end{cases} \tag{A5}$$

where θ is the incidence angle shown in figure 16. If we average (A5) over all incidence angles, then we obtain

$$\langle A \rangle \approx \frac{1}{4\pi} \int_0^{2\pi} \int_0^{\pi/2} S \cos\theta \sin\theta \, d\theta \, d\phi = S/4 \; , \tag{A6}$$

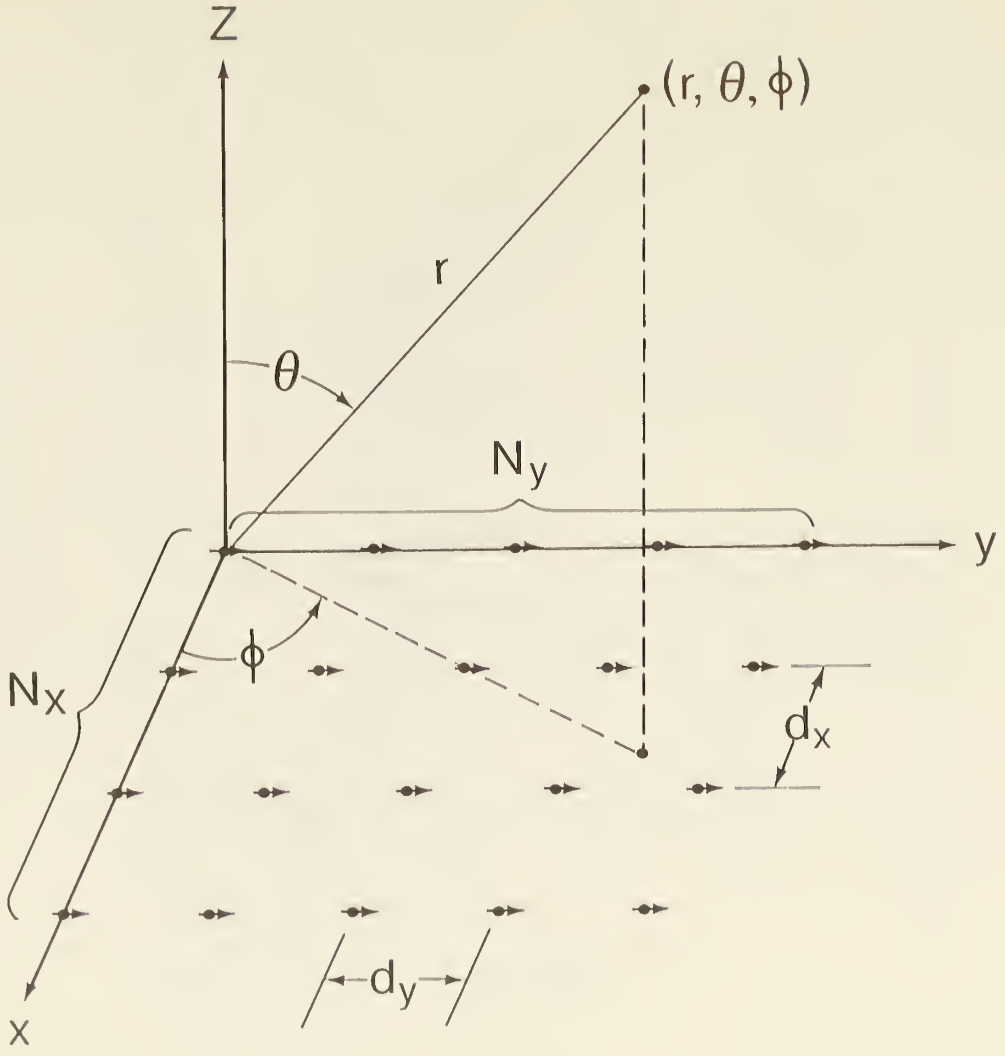
Z
(r, θ, ϕ)
r
θ
N_y
y
ϕ
N_x
d_x
d_y
x

Figure 1. Geometry for an N_x by N_y array of horizontal magnetic dipoles on a ground plane.

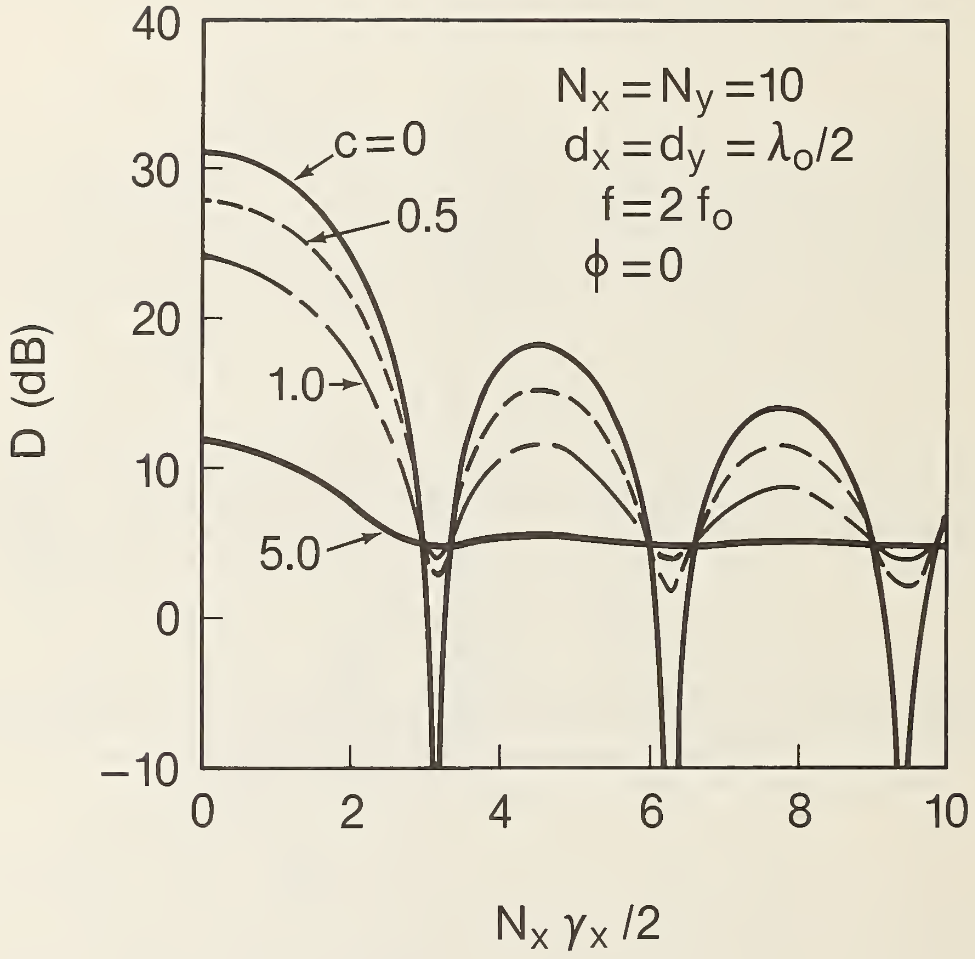

Figure 2. Directive gain D for a square array of magnetic dipole elements for various values of c.

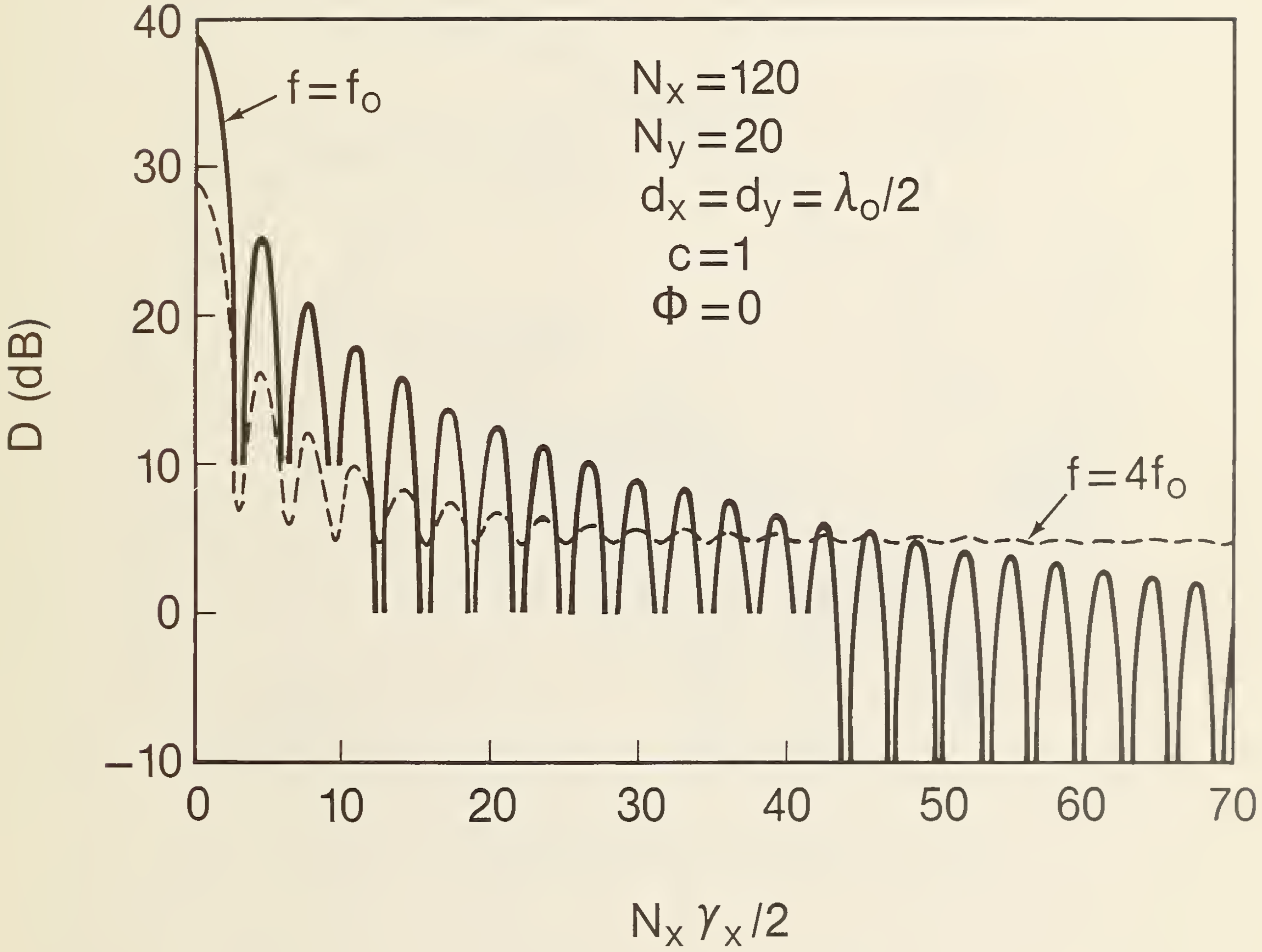

Figure 3. Directive gain for a large rectangular array of magnetic dipole elements at the design frequency f_0 and an above-band frequency $4f_0$.

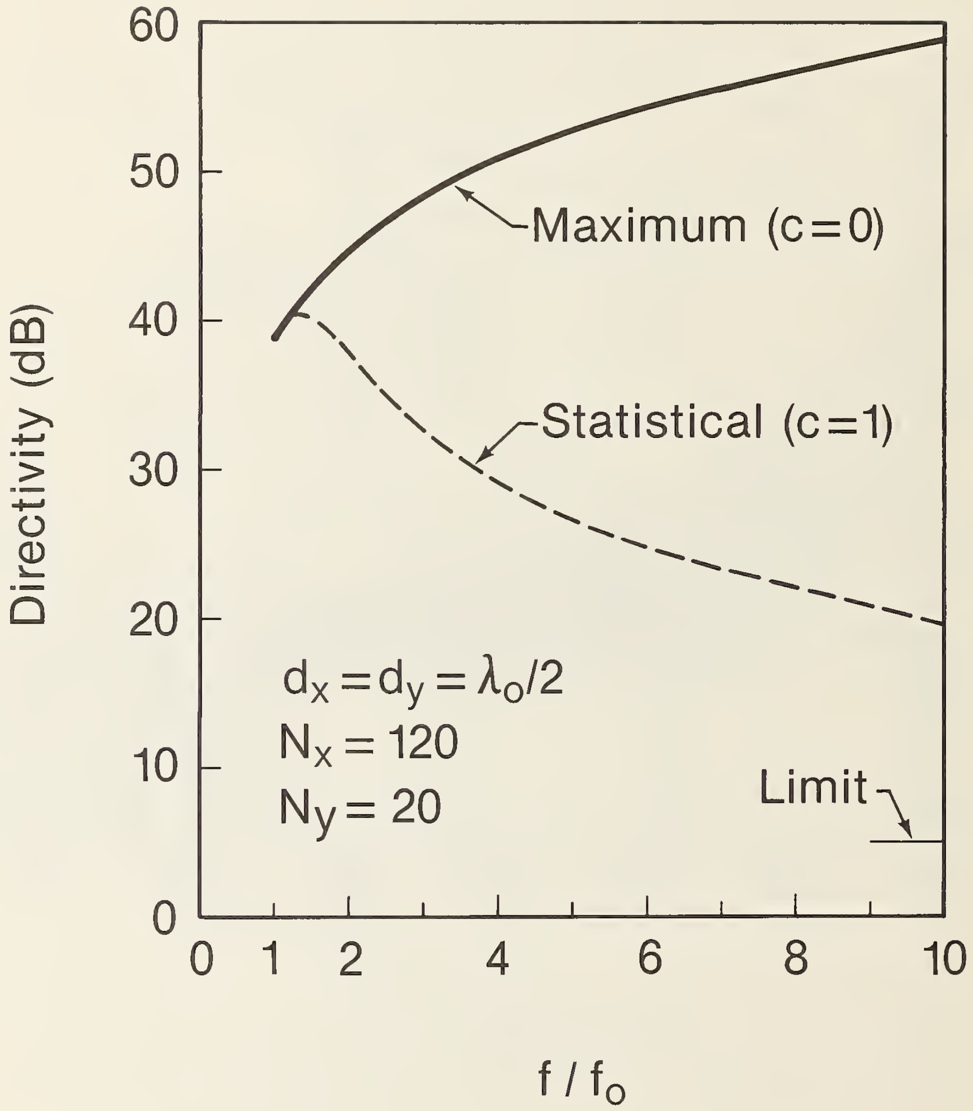

Figure 4. Directivity of a large rectangular array of magnetic dipole elements as a function of frequency.

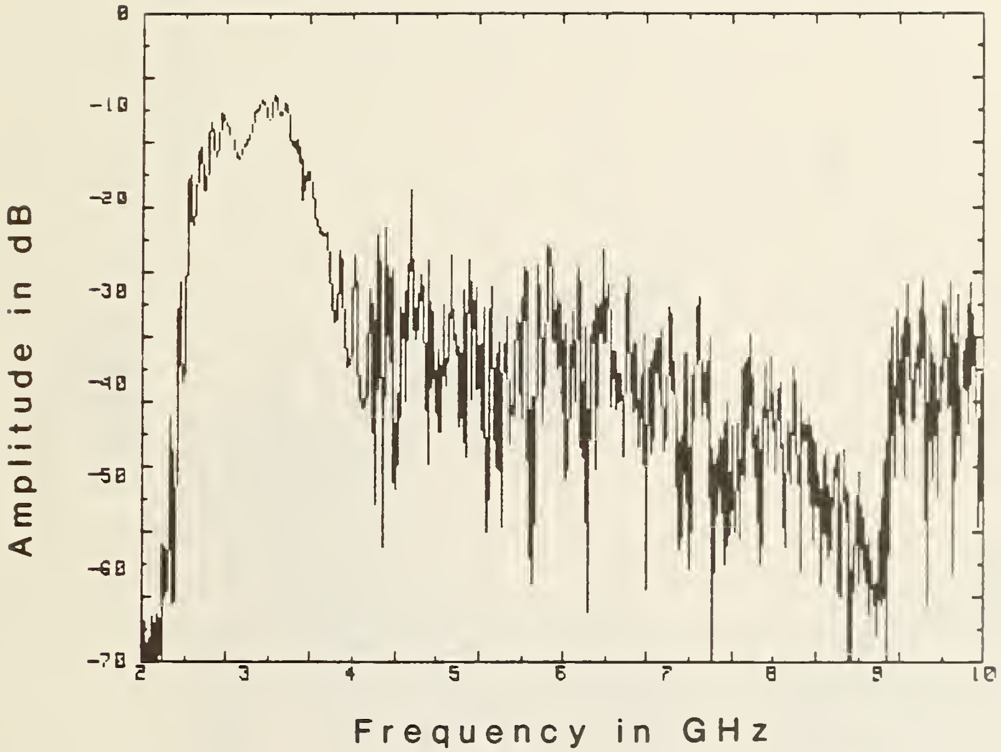

Figure 5. ULSA swept frequency response for probe at array center.

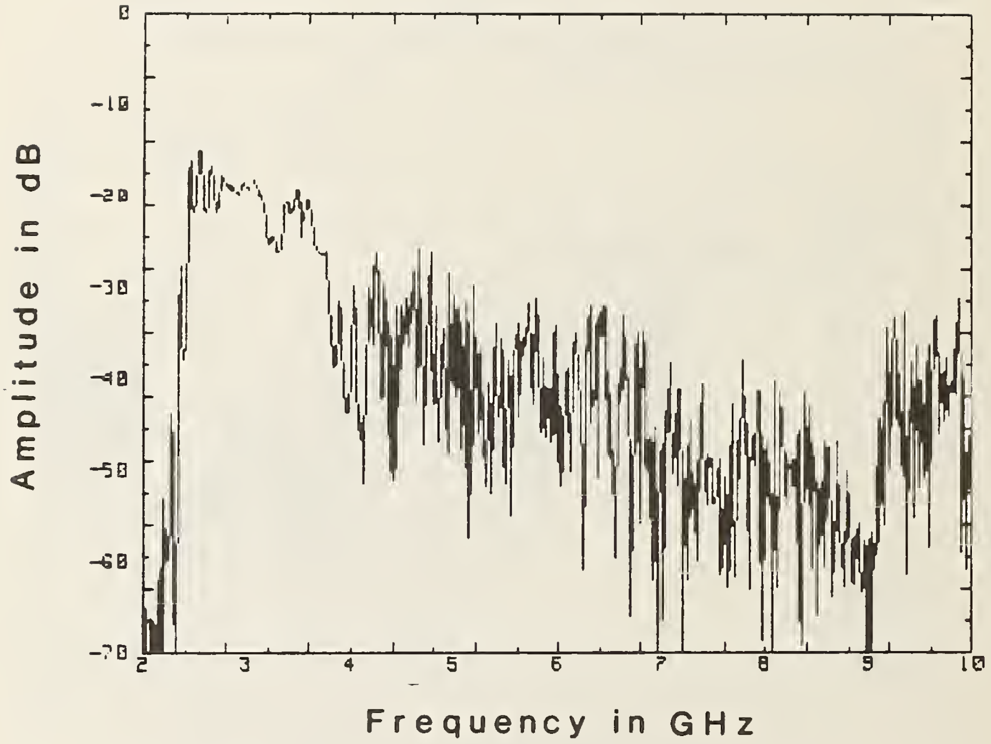

Figure 6. ULSA swept frequency response for probe 25 cm below array center.

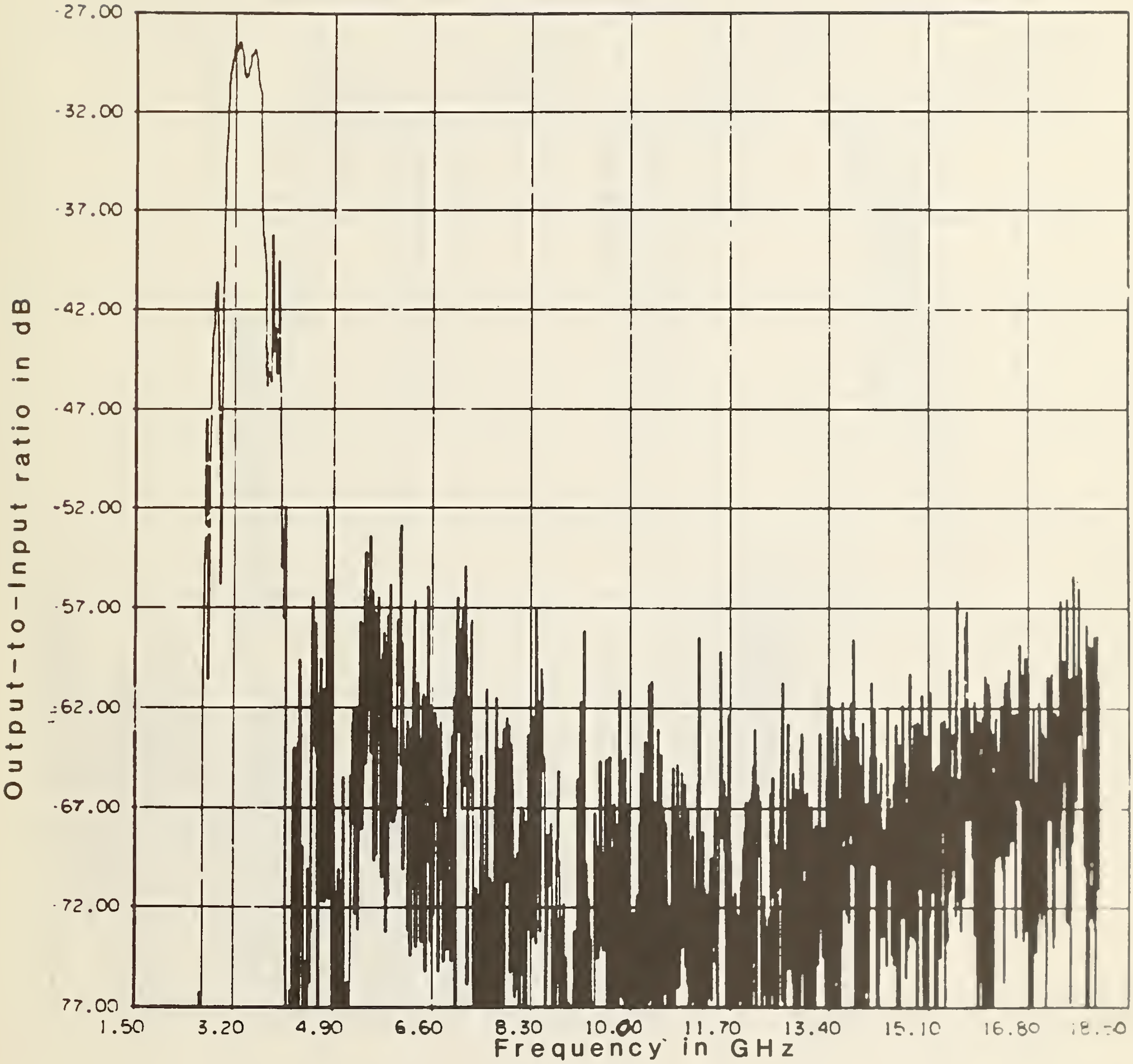

Figure 7. AWACS output-to-input ratio as a function of frequency for probe at array center.

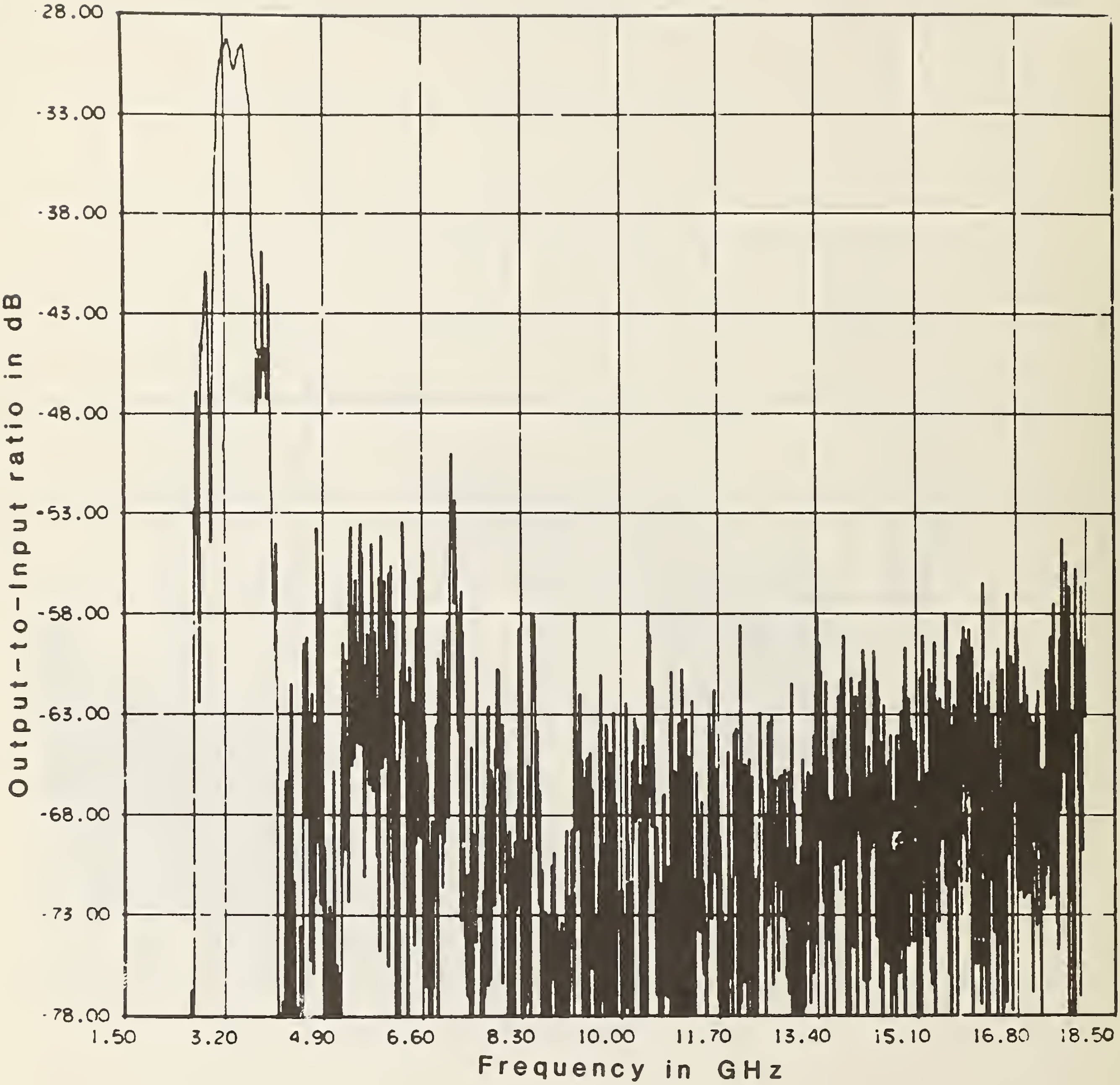

Figure 8. AWACS output-to-input ratio as a function of frequency for probe located 89 cm to the side of array center.

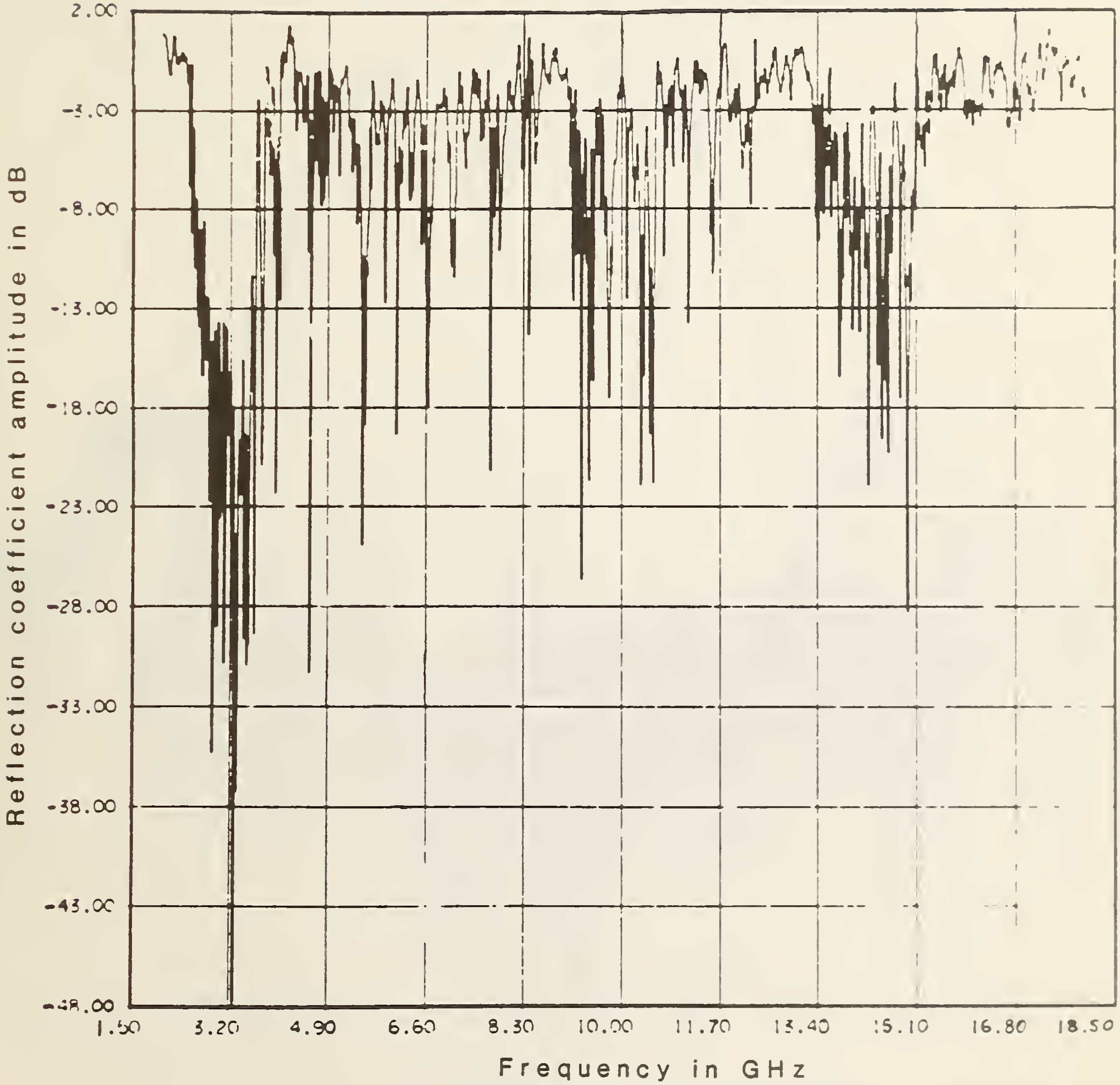

Figure 9. Amplitude of AWACS input reflection coefficient as a function of frequency.

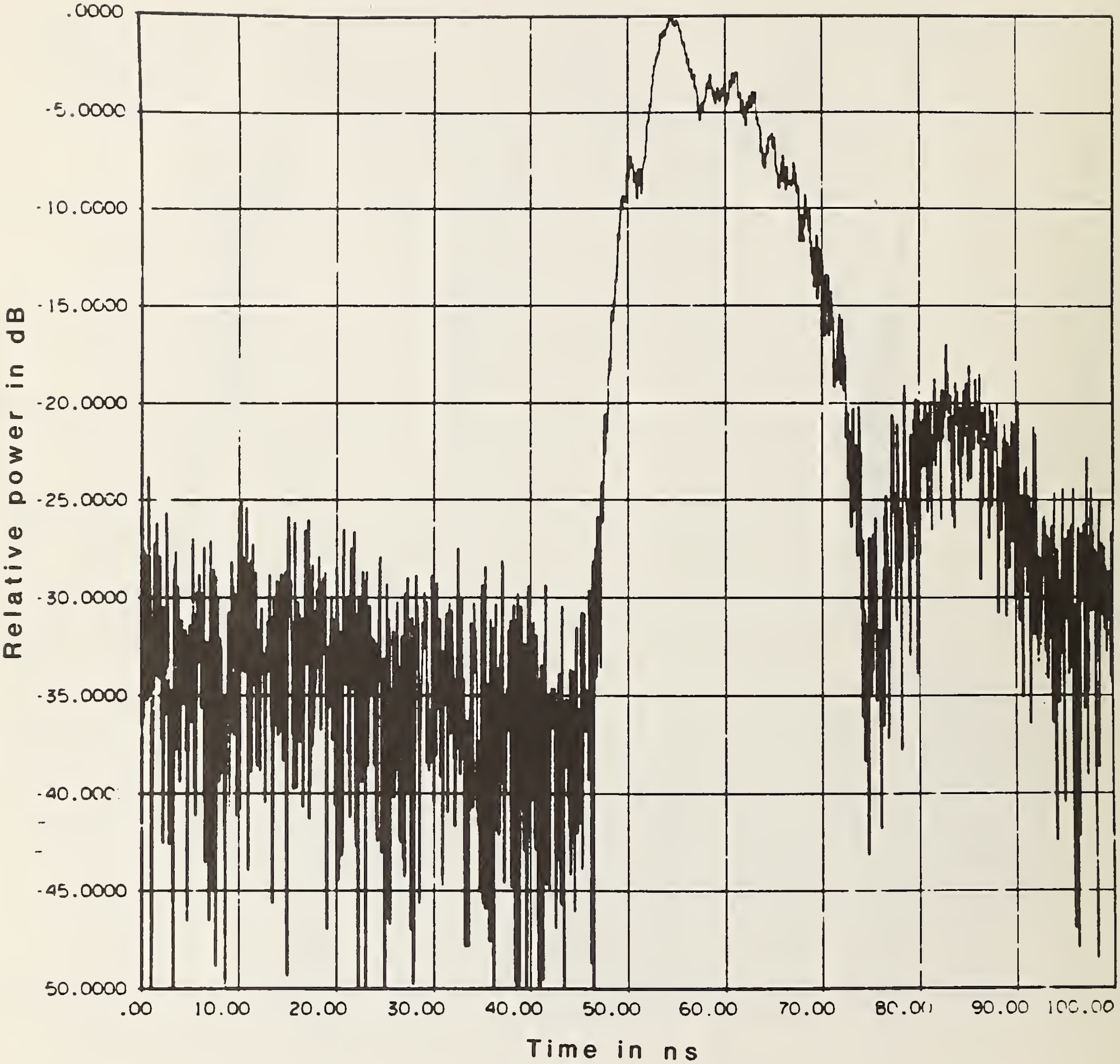

Figure 10. AWACS time domain power spectrum for probe at array center.

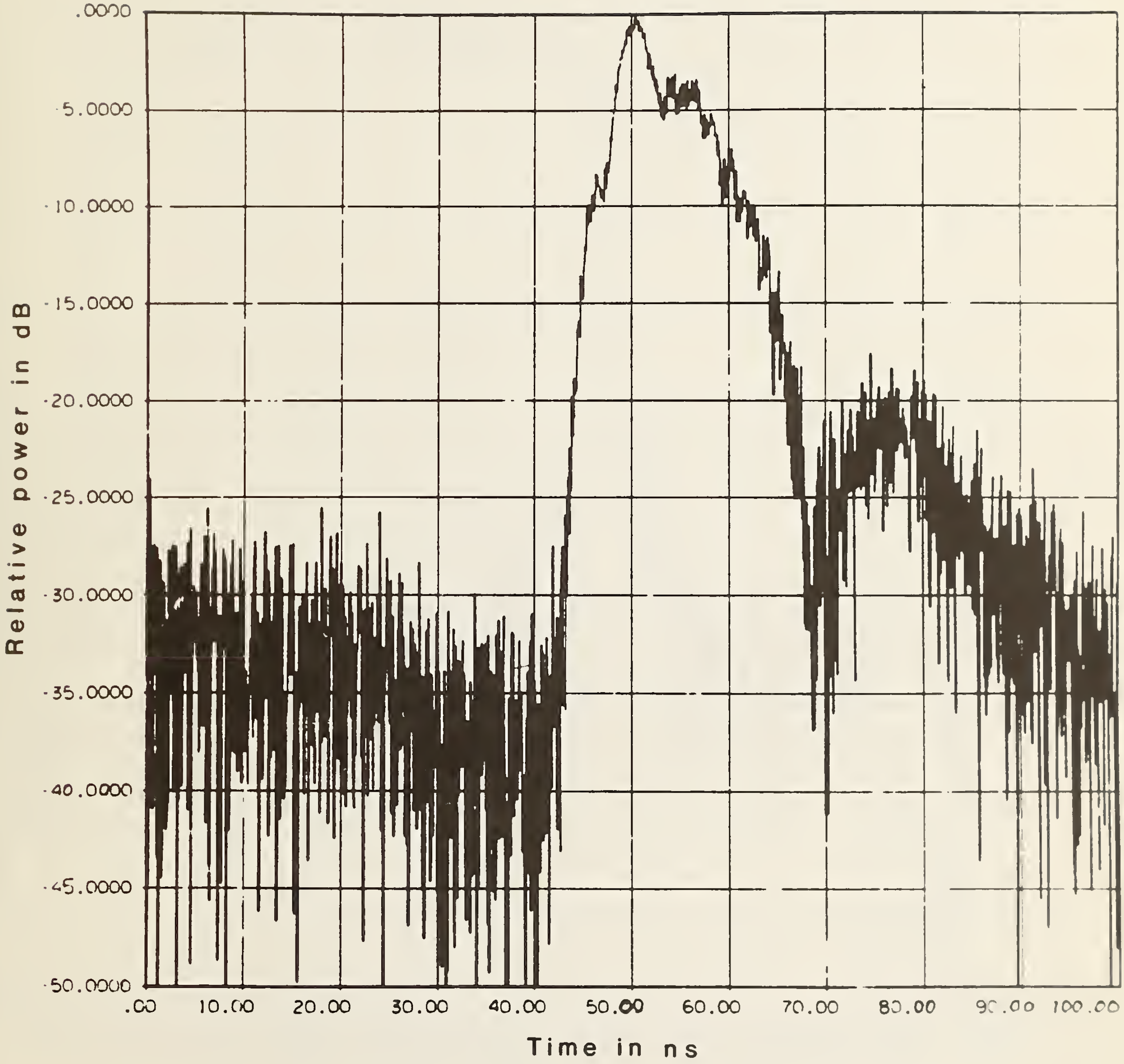

Figure 11. AWACS time domain power spectrum for probe located 89 cm to the side of array center.

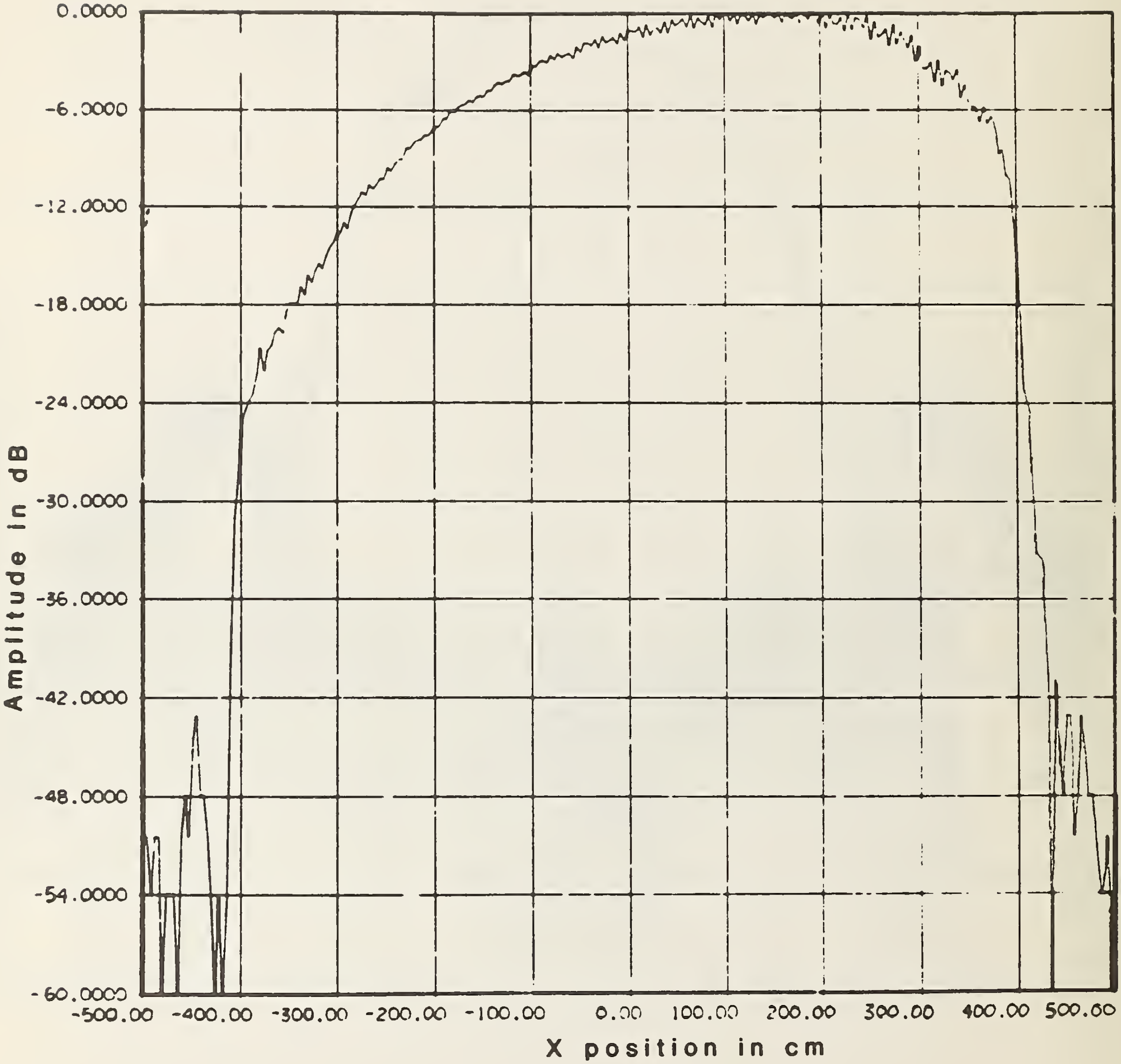

Figure 12. AWACS one-dimensional near-field x-scan at 3.94 GHz.

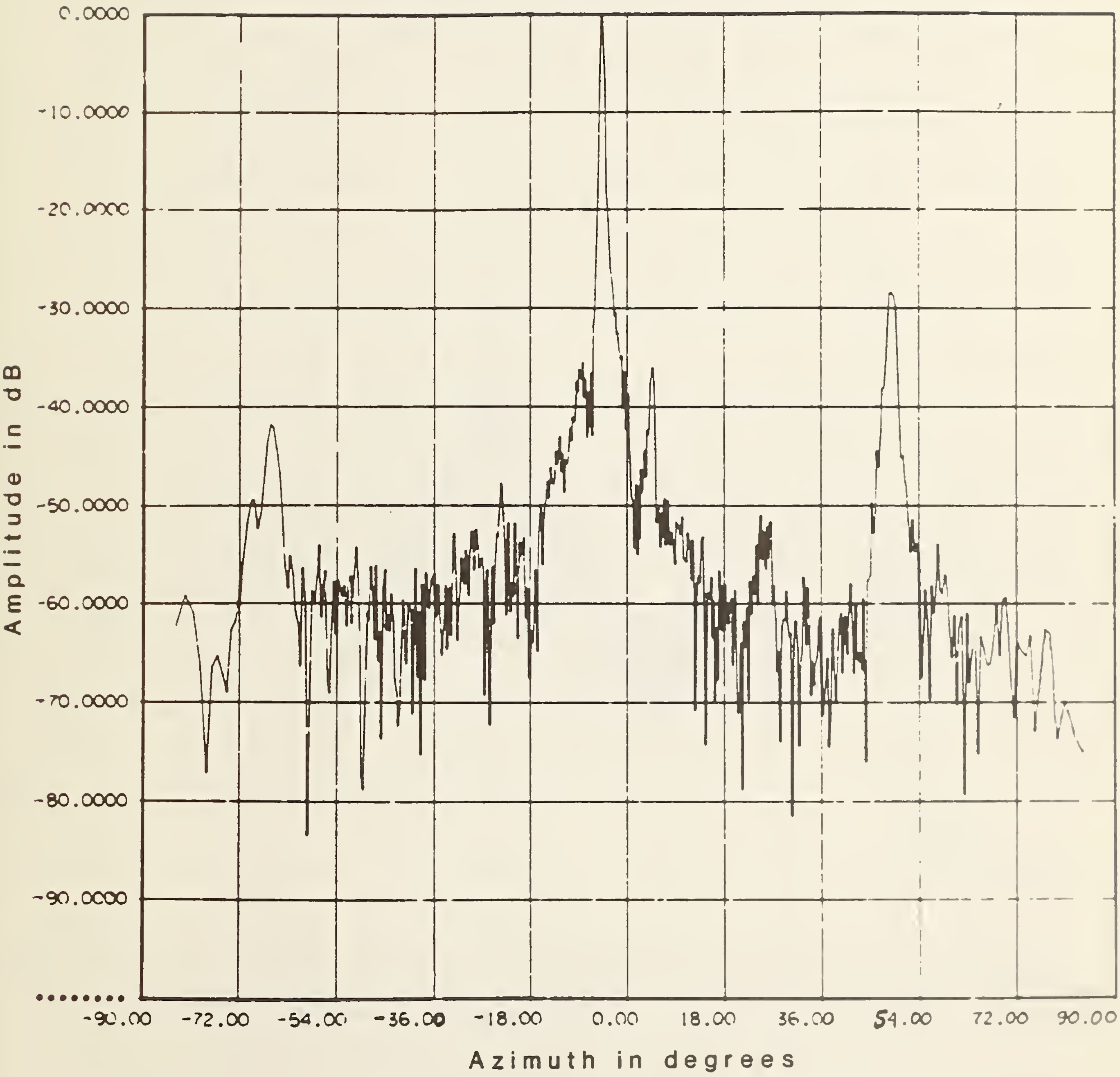

Figure 13. AWACS one-dimensional far-field x-scan at 3.94 GHZ.

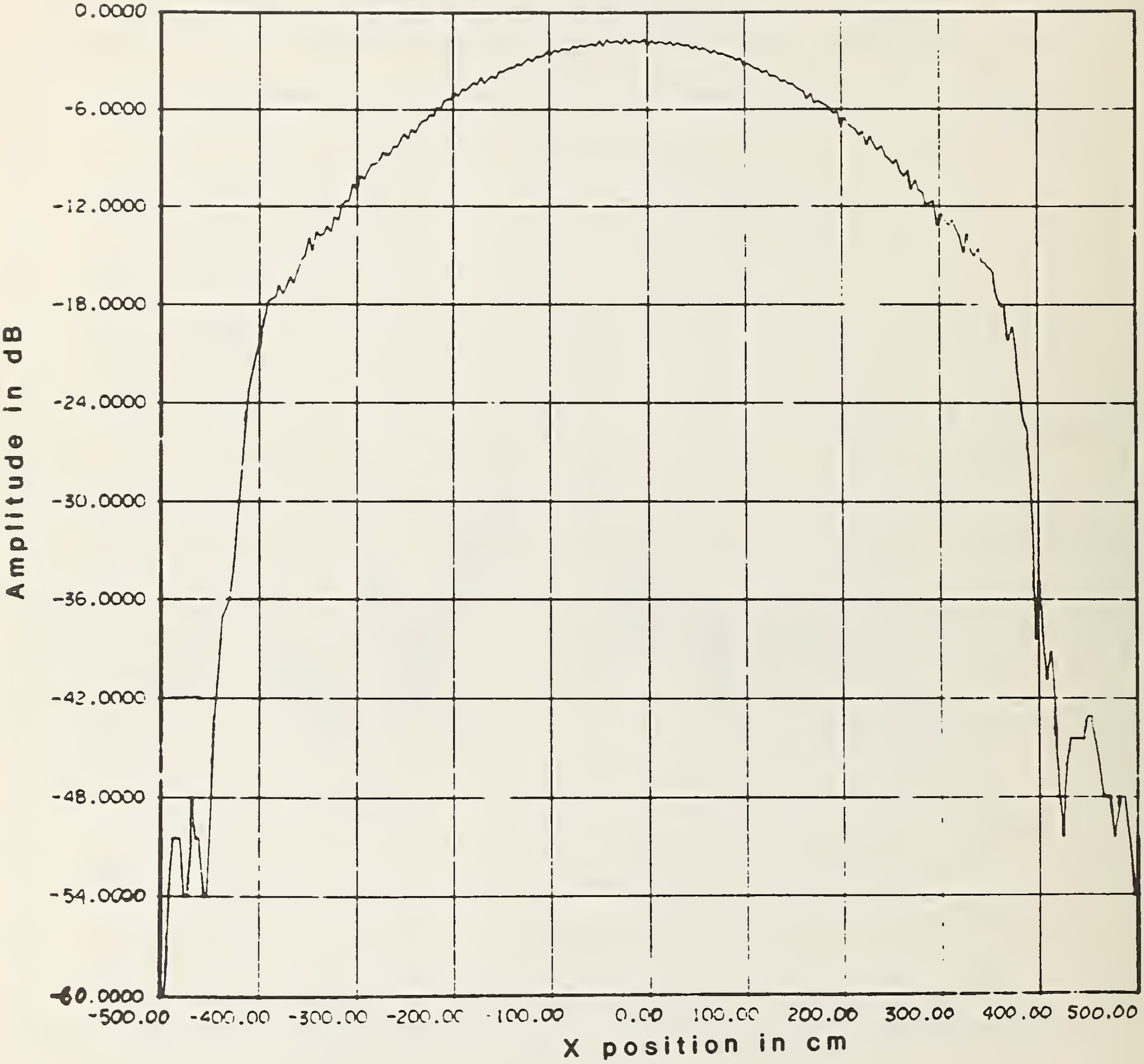

Figure 14. AWACS one-dimensional near-field x-scan at in-band frequency.

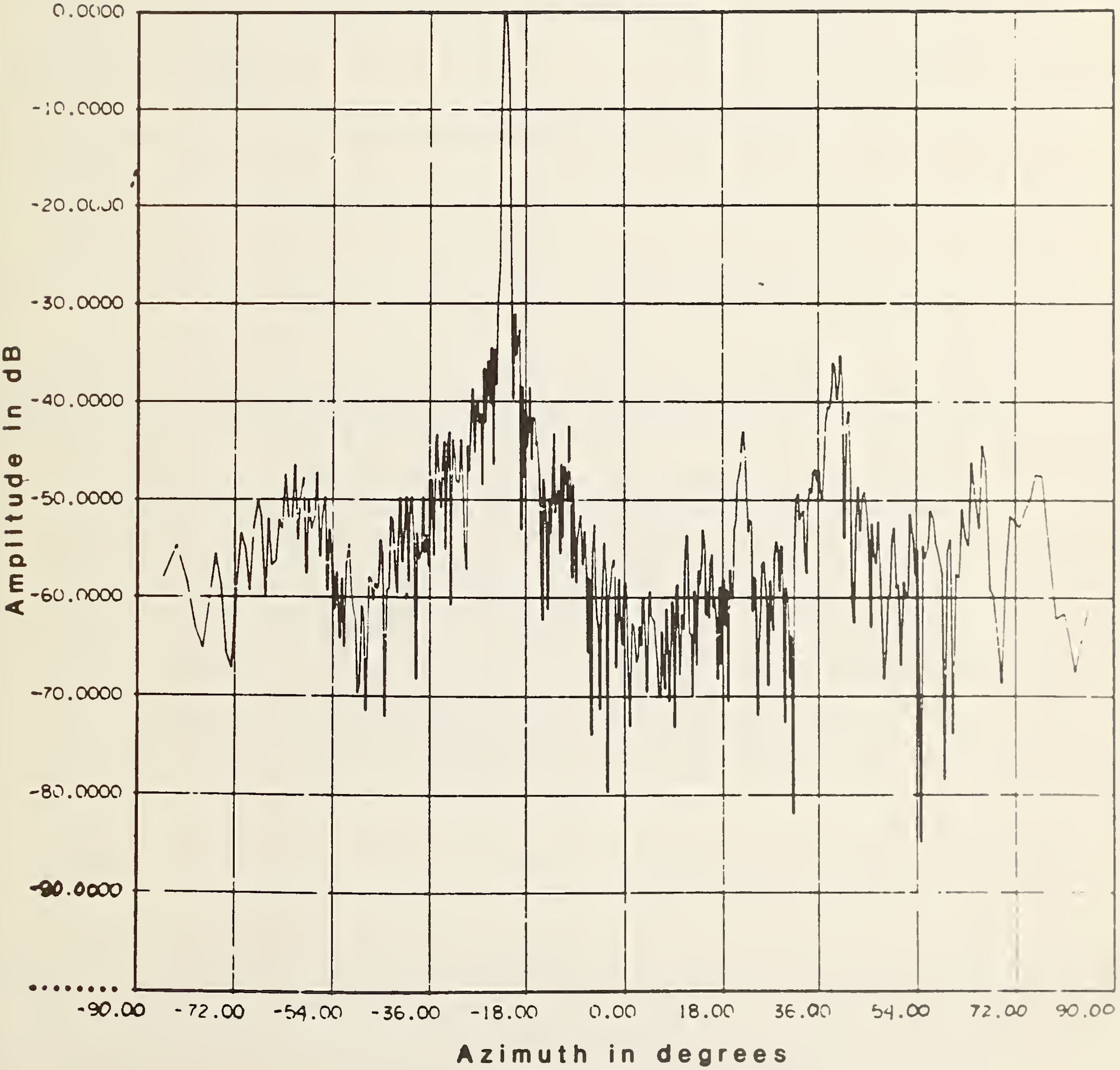

Figure 15. AWACS one-dimensional far-field x-scan at in-band frequency.

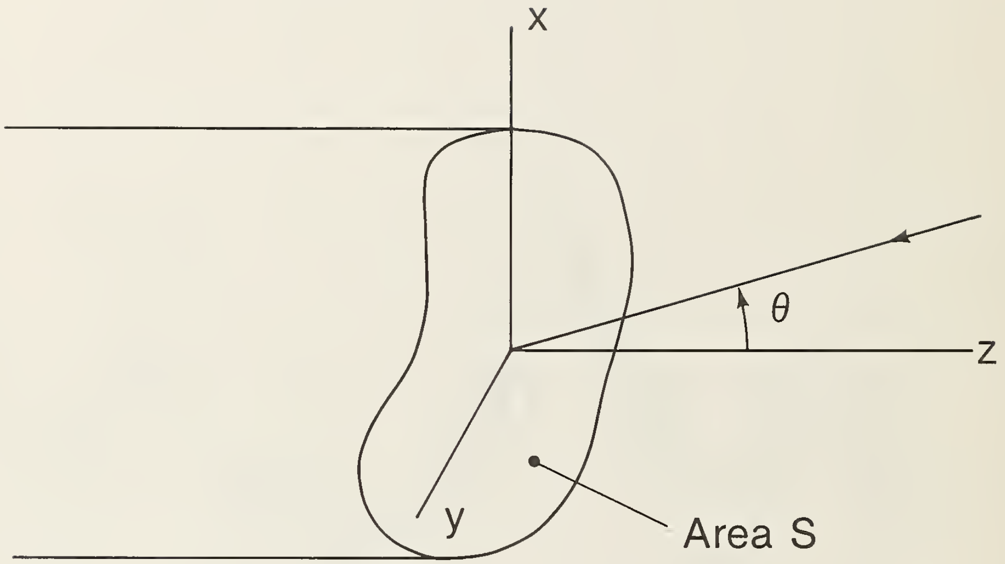

Figure 16. Open-ended waveguide of cross-sectional area S. The incident elevation angle is θ.

NBS-114A (REV. 2-80)

U.S. DEPT. OF COMM. **BIBLIOGRAPHIC DATA SHEET** *(See instructions)*	1. PUBLICATION OR REPORT NO. NBSIR 86-3047	2. Performing Organ. Report No.	3. Publication Date June 1986

4. TITLE AND SUBTITLE

Out-of-Band Response of Antenna Arrays

5. AUTHOR(S)

David A. Hill and Michael H. Francis

6. PERFORMING ORGANIZATION *(If joint or other than NBS, see instructions)*

NATIONAL BUREAU OF STANDARDS
DEPARTMENT OF COMMERCE
WASHINGTON, D.C. 20234

7. Contract/Grant No.

8. Type of Report & Period Covered

9. SPONSORING ORGANIZATION NAME AND COMPLETE ADDRESS *(Street, City, State, ZIP)*

Defense Nuclear Agency
Alexandria, Virginia 22310

10. SUPPLEMENTARY NOTES

☐ Document describes a computer program; SF-185, FIPS Software Summary, is attached.

11. ABSTRACT *(A 200-word or less factual summary of most significant information. If document includes a significant bibliography or literature survey, mention it here)*

The response of antenna arrays to out-of-band frequencies has been analyzed using the effective aperture approach. An average value of effective aperture can be obtained by averaging the incidence angle and the polarization of the incidence field. Far-field patterns have also been calculated by treating the array element excitations as random variables. The randomness in the element excitations causes a decrease in directivity and an increase in sidelobe level. Out-of-band measurements of reflection coefficient and near-field response have been made on two large slotted-waveguide arrays for frequencies from 2 to 18 GHz. Both arrays are narrow band, and this is easily explained by the large impedance mismatch at out-of-band frequencies.

12. KEY WORDS *(Six to twelve entries; alphabetical order; capitalize only proper names; and separate key words by semicolons)*

antenna array; directivity; impedance mismatch; near-field measurements; out-of-band response; polarization; slotted waveguide.

13. AVAILABILITY

☒ Unlimited
☐ For Official Distribution. Do Not Release to NTIS
☐ Order From Superintendent of Documents, U.S. Government Printing Office, Washington, D.C. 20402.
☒ Order From National Technical Information Service (NTIS), Springfield, VA. 22161

14. NO. OF PRINTED PAGES

40

15. Price

U. S. GOVERNMENT PRINTING OFFICE 1986—672 198 4 254